JOURNAL OF GUIDANCE, CONTROL, AND DYNAMICS
Vol. 25, No. 6, November–December 2002

Two-Bar Model for the Dynamics and Stability of Electrodynamic Tethers

Jesús Peláez,* Manuel Ruiz,† and Oscar López-Rebollal‡
Universidad Politécnica de Madrid, 28040 Madrid, Spain
and
Enrico C. Lorenzini§ and Mario L. Cosmo¶
Harvard–Smithsonian Center for Astrophysics, Cambridge, Massachusetts 02138

Previously a new dynamic instability that affected electrodynamic tethers in inclined orbits was studied, with a simple one-bar model that neglected the contribution of the tether lateral dynamics. The flexibility of the tether (lateral dynamics), however, plays an important role in the overall motion of the system as shown by numerical simulations of a bare-tether generator in a circular inclined orbit. The same analytical techniques of the previous work are now applied to investigate the dynamics and stability of an electrodynamic tether system modeled by two articulated bars that account for the lowest lateral modes of the tether. The analysis, which can be directly extended to any electrodynamic tether system, has been focused on two particular, but important cases: the combination of a conductive and a nonconductive leader tether (as in the Propulsive Small Expendable Deployment System) and a homogeneous, conductive tether. The lateral dynamics is extremely rich, with skip rope motion, instability peaks, and chains of bifurcations for different regions of the parameter space. The same energy pumping mechanism that destabilizes the rigid model (one bar) is found to drive an even faster instability of the lateral modes. Damping, which has not been included in the analysis, could change this unstable behavior.

Nomenclature

$A, \ldots, D$	=	coefficients in Lagrange equations
$A_0, \ldots, D_2$	=	coefficients of periodic solution
a	=	circular orbit radius
$a_1, \ldots, d_4$	=	coefficients in variational equations
B	=	stabilizing body at tether end
$\boldsymbol{B}$	=	intensity of Earth magnetic field
B_i	=	component of $\boldsymbol{B}$ along the i axis
$c\cdot$	=	cos(·)
f_{ei}	=	torque factor of current distribution, bar i
I_m	=	tether length-averaged current
I_{mi}	=	length-averaged current of tether i
i	=	orbit inclination
$\boldsymbol{i}, \boldsymbol{j}, \boldsymbol{k}$	=	unit vectors of the orbital frame
$\boldsymbol{J}_A$	=	inertia diadic of a bar at point A
K_0	=	coefficient in variational equations
k	=	component of oscillation eigenvalues
L	=	total tether length
$\mathcal{L}$	=	tethered system Lagrangian function
L_i	=	length of bar i
M	=	monodromy matrix
m_B	=	end mass at point B
m_i	=	mass of bar i, $i = 1, 2$
m_T	=	tether total mass
O	=	main spacecraft
Q_i	=	generalized force for q_i
q_i	=	generalized coordinate i
$s\cdot$	=	sin(·)
T	=	articulation point of bars 1 and 2
$\boldsymbol{u}_i$	=	unit vector along bar i
$\boldsymbol{u}_m$	=	direction vector of the magnetic dipole
$\boldsymbol{y}$	=	vector of generalized coordinates
$\boldsymbol{y}_p$	=	periodic solution vector
δ_i	=	mass ratio of bar i, m_i/m_B
ϵ_i	=	electrodynamic to gravity gradient force ratio for bar i
$\boldsymbol{\eta}$	=	vector of perturbed generalized coordinates
θ_i	=	pitch angle of bar i
Λ	=	length ratio of the two bars
Λ^*	=	critical length ratio of the two bars
λ_i	=	eigenvalues of the Monodromy matrix
μ	=	Earth gravitational constant
μ_m	=	Earth magnetic dipole
ν	=	orbit anomaly ωt
σ	=	coefficient of ϵ^3 in the eigenvalues expansion
φ_i	=	roll angle of bar i
ω	=	circular orbit frequency
$\boldsymbol{\omega}$	=	angular speed of a solid
ω_i	=	tether oscillation frequencies, $i = 1, \ldots, 4$
ω_i^*	=	tether critical oscillation frequencies

Superscripts

$\cdot$	=	$\mathrm{d}(\,)/\mathrm{d}\nu$
$\cdot\cdot$	=	$\mathrm{d}^2(\,)/\mathrm{d}\nu^2$

Introduction

THERE is a renewed interest in electrodynamic tethers for space propulsion, deorbiting, and power generation. Different concepts are being studied to build a deorbiting tether system combining safety, reliability, speed, and low cost. Significant electrodynamic thrust must be obtained with a light tether system.[1–4] The most promising technology is a thin bare tether anode that collects electrons from the ionosphere with greater efficiency than the classical approach of a large spherical termination.[5,6] However, simulations

Received 18 June 2001; revision received 7 February 2002; accepted for publication 8 May 2002.

*Associate Professor, Escuela Técnica Superior de Ingenieros Aeronáuticos, Pl. Cardenal Cisneros, 3; jpelaez@faia.upm.es.

†Associate Professor, Escuela Técnica Superior de Ingenieros Aeronáuticos, Pl. Cardenal Cisneros, 3; mrd@faia.upm.es.

‡Associate Professor, Escuela Técnica Superior de Ingenieros Aeronáuticos, Pl. Cardenal Cisneros, 3; oscar@faia.upm.es.

§Staff Scientist, Head of Special Projects Group, Radio and Geoastronomy Division, 60 Garden Street; elorenzini@cfa.harvard.edu. Senior Member AIAA.

¶Staff Scientist, Special Projects Group, Radio and Geoastronomy Division, 60 Garden Street; mcosmo@cfa.harvard.edu.

of electrodynamic tether dynamics show a very complex motion with strong couplings and energy transfers between different vibration modes.[2,7]

High thrust or drag requires a high current in the wire. Current intensity depends on environmental conditions: plasma density, magnetic field, and tether temperature. The frequency spectrum of the electrodynamic forces thus concentrates on low frequencies, and they should excite mainly the low-frequency dynamic modes of the system. However, they turn out to excite the higher frequency modes of the system as well.[2] The dynamics is particularly interesting for systems following inclined orbits, where a strong skip rope motion develops. The bent tether moves about the line through the end masses, which is itself moving. The strong lateral motion affects the performance of the system and, for certain conditions, its overall dynamic stability.[2,7]

Recently Peláez et al. have identified a mechanism destabilizing the system dynamics on inclined orbits that had not been considered before.[8] An important instability analyzed by Levin[9] and Beletsky and Levin,[10] for equatorial orbits and a nontilted dipole model, was due to coupling between elastic longitudinal oscillations and in-plane libration. This new mechanism is even more basic because it involves the loss of stability of an equilibrium position that is independent of elasticity. When there is no current, the local vertical is a stable equilibrium configuration. In an equatorial orbit with an idealized nontilted dipole model, the magnetic field is normal to the orbital plane, and the current produces a force normal to the tether in the orbital plane. The equilibrium position moves forward (with thrust) or backward (with drag). In inclined orbits or on equatorial orbits with a realistic magnetic field, there are periodic components of the magnetic field along the local vertical and normal to the orbit plane. The equilibrium position gives way to a periodic motion, which was found to be unstable.[8]

The magnetic field component along the local vertical causes an inclination-dependent coupling between in-plane and out-of-plane librations. The component of the magnetic field normal to the orbit plane produces a force that ends up continuously pumping energy into the system, which eventually becomes unstable. The destabilization mechanism for a straight tether model was analyzed in Ref. 8. Note that the instability takes place even in the absence of force components resonating with the natural librations of the system.

The previous study considered the tether as a rigid bar and, thus, did not include the lateral dynamics of the tether. In this paper, we analyze the influence of tether lateral dynamics on the system stability. We consider two different cases: 1) an electrodynamic tether with a continuous conductive wire connecting the two end bodies and 2) a Propulsive Small Expendable Deployment System-(ProSEDS-) like tether configuration with a conductive wire of some length, followed by a nonconductive tether that provides additional dynamic stabilization.[4] In both cases, we use a simple model with two articulated bars to describe the lateral dynamics of the tether. The electrodynamic forces model is also simple: a nontilted magnetic dipole and constant current. Nevertheless, it leads to the formulation of a few conclusions of general validity.

Description of the Model

A massive spacecraft O follows a circular orbit of radius a, angular frequency $\omega = \sqrt{(\mu/a^3)}$, and inclination i. A tether of mass m_T with an end mass m_B is attached to the spacecraft. Their masses are negligible compared with that of O, so that the orbit is unperturbed and the center of mass of the system stays at O. $Oxyz$ is the orbital frame, with Ox along the local vertical toward zenith, Oy normal to the orbit plane and opposite to the orbital angular momentum, and Oz along the flight direction.

We model the tether as two rigid bars articulated at T, $\overrightarrow{OT}$ and $\overrightarrow{TB}$, whose masses and lengths are m_1 and L_1 and m_2 and L_2, respectively. The total mass of the tether is $m_T = m_1 + m_2$, and the total length $L = L_1 + L_2$. The end mass B is modeled as a point mass m_B.

The position of each bar in the orbital frame is given by the in-plane angles θ_1 and θ_2 and the out-of-plane angles φ_1 and φ_2, as shown in Fig. 1. Throughout the paper and for the sake of brevity, we will use the notation $cx = \cos x$ and $sx = \sin x$.

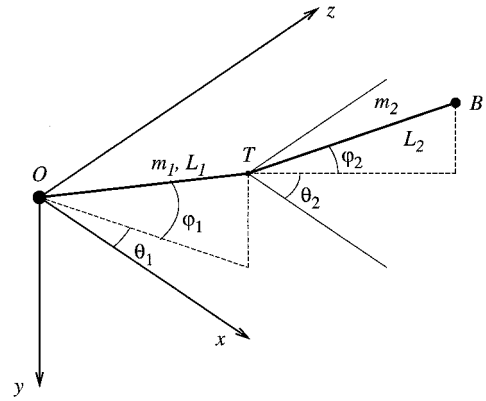

Fig. 1 Orbital frame and tether angles.

Earth Gravity Model and Inertia Forces

The Earth's gravity is assumed spherical, and, consequently, the orbital plane will remain steady in the inertial geocentric frame $Ex_1y_1z_1$. Because $L \ll a$, the gravitational potential is linearized in the neighborhood of the circular orbit, neglecting terms smaller than $(L/a)^2$:

$$V_g = -\omega^2[a^2 - xa + (2x^2 - y^2 - z^2)/2]$$

Let $\boldsymbol{x}$ be the position of a point mass relative to a moving frame of angular speed $\boldsymbol{\omega}$, whose origin has an acceleration $\boldsymbol{\gamma}^O$. Landau and Lifshitz[11] showed that the inertia forces derive from a velocity-dependent potential:

$$V_i = \boldsymbol{\gamma}^O \cdot \boldsymbol{x} - (\boldsymbol{\omega} \wedge \boldsymbol{x})^2/2 - \boldsymbol{\omega} \cdot (\boldsymbol{x} \wedge \dot{\boldsymbol{x}})$$

In the case of a circular orbit, $\boldsymbol{\gamma}^O = -\omega^2 a\boldsymbol{i}$ and $\boldsymbol{\omega} = -\omega\boldsymbol{j}$, leading to

$$V_i = -\omega^2(2ax + z^2 + x^2)/2 + \omega(z\dot{x} - x\dot{z})/2$$

The inertia and linearized gravity forces together give the gravity-gradient force. Thus, the acceleration of a point mass of coordinates $\boldsymbol{x} = (x, y, z)$ in the orbital frame is given by

$$\boldsymbol{f} = \omega^2(3x\boldsymbol{i} - y\boldsymbol{j}) + 2\omega(\dot{z}\boldsymbol{i} - \dot{x}\boldsymbol{k})$$

Earth Magnetic Field

The Earth magnetic field $\boldsymbol{B}$ is modeled by means of a dipole whose axis is defined by the unit vector $\boldsymbol{u}_m$. Let $\boldsymbol{r} = r\boldsymbol{u}_r$ be the position vector of a given point P in the geocentric frame, then the field $\boldsymbol{B}$ in P is

$$\boldsymbol{B}(\boldsymbol{r}) = \left(\mu_m / r^3\right)[\boldsymbol{u}_m - 3\,(\boldsymbol{u}_m \cdot \boldsymbol{u}_r)\,\boldsymbol{u}_r] \tag{1}$$

where μ_m is the strength of the dipole.[12] In a tilted dipole model, the unit vector $\boldsymbol{u}_m$ would rotate around the Earth's spin axis; here we adopt a nontilted dipole model because the tilt is not essential in explaining the instability mechanism. Therefore, the components (B_x, B_y, B_z) in the orbital frame are

$$B_x = -\left(2\mu_m/a^3\right)sisv, \qquad B_y = -\left(\mu_m/a^3\right)ci$$

$$B_z = +\left(\mu_m/a^3\right)sicv$$

where v is the true anomaly of the orbit with origin at the ascending node.

Electrodynamics Forces

Our analysis can be applied both to the classical configuration with an end collector and to the bare tether collector. When used as a generator or brake, the tether collects electrons from the ionosphere, which are then ejected back into the ionosphere by the cathodic contactor at the lower end. Thus, electric current flows from the lower to the higher end of the tether. In the thruster mode, the current is forced to flow in the opposite direction by means of a power supply that biases the tether positively with respect to the ambient plasma. For a bare tether, current varies linearly along the tether. For an insulated, end-collector tether, current is constant along the tether.

The electrodynamic force acting on a tether element of length $\mathrm{d}s$, current $I(s)$, and tangent vector $\boldsymbol{u}_1$ is $\boldsymbol{f}_e\,\mathrm{d}s = I(s)\,\mathrm{d}s\,\boldsymbol{u}_1 \times \boldsymbol{B}$, where s is the distance from O. For a rigid tether, the system of distributed forces is equivalent to a resultant force and torque applied at the articulation point and given by

$$\boldsymbol{F}_e = I_m L \boldsymbol{u}_1 \times \boldsymbol{B}, \qquad \boldsymbol{M}_e = f_e I_m L^2\, \boldsymbol{u}_1 \times (\boldsymbol{u}_1 \times \boldsymbol{B})$$

This is done for each segment of the tether. Here I_m is the average current along the wire, and the factor f_e shows the effect of current distribution on the torque:

$$L I_m = \int_0^L I(s)\,\mathrm{d}s, \qquad f_e I_m L^2 = \int_0^L sI(s)\,\mathrm{d}s$$

where f_e is $\frac{1}{2}$ for an insulated tether (uniform current), $\frac{2}{3}$ for a bare tether with current falling to zero at the tip, and $\frac{1}{6}$ for a bare tether with zero current at the origin with $I_m > 0$ for the generator mode and $I_m < 0$ for the thruster mode.

Equations of Motion

The Lagrangian function is computed as in Ref. 8, taking θ_1, φ_1, θ_2, and φ_2 as generalized coordinates and true anomaly ν as the independent variable. We compute first the kinetic energy of the system in the motion relative to the orbital frame. The first bar is treated as a solid with a fixed point: $\boldsymbol{\omega}\cdot\boldsymbol{J}_O\cdot\boldsymbol{\omega}/2$. Koenig's theorem is applied to the second one, to obtain $m_2\boldsymbol{v}_G^2/2 + \boldsymbol{\omega}\cdot\boldsymbol{J}_G\cdot\boldsymbol{\omega}/2$; whereas that of the end mass is trivial. Gravitational and inertial potential are integrated over the two bars and computed for the end mass. The Lagrangian function thus obtained is

$$\begin{aligned}
\mathcal{L} = {} & \tfrac{1}{6}(m_2+3m_B)\omega^2 L_2^2\left\{\dot\varphi_2^2 + c^2\varphi_2\left[(1+\dot\theta_2)^2 + 3c^2\theta_2\right]\right\} \\
& + \tfrac{1}{6}(m_1+3m_2+3m_B)\omega^2 L_1^2\left\{\dot\varphi_1^2 + c^2\varphi_1\left[(1+\dot\theta_1)^2 + 3c^2\theta_1\right]\right\} \\
& + \tfrac{1}{2}(m_2+2m_B)\omega^2 L_1 L_2\left\{c\varphi_1 c\varphi_2 c(\theta_2-\theta_1)(\dot\theta_1\dot\theta_2 + \dot\theta_1 + \dot\theta_2)\right. \\
& - c\varphi_1 s\varphi_2 s(\theta_2-\theta_1)\dot\varphi_2(\dot\theta_1+1) + s\varphi_1 c\varphi_2 s(\theta_2-\theta_1)\dot\varphi_1(\dot\theta_2+1) \\
& + \left[c\varphi_1 c\varphi_2 + s\varphi_1 s\varphi_2 c(\theta_2-\theta_1)\right]\dot\varphi_1\dot\varphi_2 \\
& \left. + 3c\varphi_1 c\varphi_2 c\theta_1 c\theta_2 - s\varphi_1 s\varphi_2\right\}
\end{aligned}$$

This could also be done by computing the kinetic energy of the absolute motion in inertial axes, in terms of the earlier given coordinates and derivatives, plus the linearized gravitational potential, without the inertial potential. This leads to a different Lagrangian function, but the Lagrange equations are the same: The contribution of the difference to each equation is zero.

Electrodynamic forces do not derive from a potential, and they must be included as generalized forces. The work of the electromagnetic forces and torques on each bar is computed for each coordinate's virtual displacement δq_i, leading to

$$\begin{aligned}
Q_{\theta_1} = {} & +f_{e_1} I_{m_1} L_1^2 c\varphi_1\{s\varphi_1(B_x c\theta_1 + B_z s\theta_1) + B_y c\varphi_1\} \\
& + I_{m_2} L_1 L_2 c\varphi_1\{s\varphi_2(B_x c\theta_1 + B_z s\theta_1) + B_y c\varphi_2 c(\theta_2-\theta_1)\} \\
Q_{\varphi_1} = {} & -f_{e_1} I_{m_1} L_1^2\{B_x s\theta_1 - B_z c\theta_1\} + I_{m_2} L_1 L_2\{B_y c\varphi_2 s\varphi_1 s(\theta_2-\theta_1) \\
& - \{B_x s\theta_1 - B_z c\theta_1\} s\varphi_1 s\varphi_2 - \{B_x s\theta_2 - B_z c\theta_2\} c\varphi_1 c\varphi_2\} \\
Q_{\theta_2} = {} & +f_{e_2} I_{m_2} L_2^2 c\varphi_2\{s\varphi_2(B_x c\theta_2 + B_z s\theta_2) + B_y c\varphi_2\} \\
Q_{\varphi_2} = {} & -f_{e_2} I_{m_2} L_2^2\{B_x s\theta_2 - B_z c\theta_2\}
\end{aligned}$$

When the nondimensional parameters are introduced,

$$\Lambda = \frac{L_1}{L}, \qquad \delta_1 = \frac{m_1}{m_B}, \qquad \delta_2 = \frac{m_2}{m_B}$$

$$\varepsilon_1 = \frac{3 f_{e_1} I_{m_1}}{m_T + 3m_B}\cdot\frac{\mu_m}{\mu}, \qquad \varepsilon_2 = \frac{3 f_{e_2} I_{m_2}}{m_T + 3m_B}\cdot\frac{\mu_m}{\mu}$$

The Lagrange equations can be written as

$$\begin{aligned}
& Ac\varphi_1\ddot\theta_1 + \tfrac{3}{2}Bc(\theta_2-\theta_1)c\varphi_2\ddot\theta_2 - \tfrac{3}{2}Bs(\theta_2-\theta_1)s\varphi_2\ddot\varphi_2 \\
& \quad - 2As\varphi_1\dot\varphi_1(1+\dot\theta_1) - 3Bs\varphi_2 c(\theta_2-\theta_1)\dot\varphi_2(1+\dot\theta_2) \\
& \quad - \tfrac{3}{2}Bs(\theta_2-\theta_1)c\varphi_2\left(\dot\theta_2^2 + 2\dot\theta_2 + \dot\varphi_2^2\right) + s\theta_1\left(3Ac\theta_1 c\varphi_1\right. \\
& \quad \left. + \tfrac{9}{2}Bc\theta_2 c\varphi_2\right) + \varepsilon_1\Lambda C\{sis\varphi_1(2c\theta_1 s\nu - s\theta_1 c\nu) \\
& \quad + cic\varphi_1\} + (\varepsilon_2/f_{e_2})C(1-\Lambda)\{sis\varphi_2(2c\theta_1 s\nu - s\theta_1 c\nu) \\
& \quad + cic\varphi_2 c(\theta_2-\theta_1)\} = 0
\end{aligned} \tag{2}$$

$$\begin{aligned}
& A\ddot\varphi_1 + \tfrac{3}{2}Bs(\theta_2-\theta_1)s\varphi_1 c\varphi_2\ddot\theta_2 + \tfrac{3}{2}B\{c\varphi_1 c\varphi_2 \\
& \quad + s\varphi_1 s\varphi_2 c(\theta_2-\theta_1)\}\ddot\varphi_2 + \tfrac{3}{2}Bc(\theta_2-\theta_1)s\varphi_1 c\varphi_2\left(\dot\theta_2^2 + 2\dot\theta_2 + \dot\varphi_2^2\right) \\
& \quad + As\varphi_1 c\varphi_1\dot\theta_1(2+\dot\theta_1) - 3Bs(\theta_2-\theta_1)s\varphi_1 s\varphi_2\dot\varphi_2(1+\dot\theta_2) \\
& \quad - \tfrac{3}{2}Bs\varphi_2 c\varphi_1\dot\varphi_2^2 - \varepsilon_1\Lambda Csi\,(c\theta_1 c\nu + 2s\theta_1 s\nu) \\
& \quad - (\varepsilon_2/f_{e_2})C(1-\Lambda)\{sis\varphi_1 s\varphi_2(c\theta_1 c\nu + 2s\theta_1 s\nu) \\
& \quad + sic\varphi_1 c\varphi_2(c\theta_2 c\nu + 2s\theta_2 s\nu) - cis(\theta_2-\theta_1)s\varphi_1 c\varphi_2\} \\
& \quad + c\varphi_1\left(\tfrac{3}{2}Bs\varphi_2 + As\varphi_1\right) + s\varphi_1 c\theta_1\left(\tfrac{9}{2}Bc\theta_2 c\varphi_2\right. \\
& \quad \left. + 3Ac\theta_1 c\varphi_1\right) = 0
\end{aligned} \tag{3}$$

$$\begin{aligned}
& \tfrac{3}{2}Dc\varphi_1 c(\theta_2-\theta_1)\ddot\theta_1 + \tfrac{3}{2}Ds\varphi_1 s(\theta_2-\theta_1)\ddot\varphi_1 - Ec\varphi_2\ddot\theta_2 \\
& \quad + \tfrac{3}{2}Dc\varphi_1 s(\theta_2-\theta_1)\left(\dot\theta_1^2 + 2\dot\theta_1 + \dot\varphi_1^2\right) \\
& \quad - 3Ds\varphi_1 c(\theta_2-\theta_1)\dot\varphi_1(1+\dot\theta_1) + 2Es\varphi_2\dot\varphi_2(1+\dot\theta_2) \\
& \quad - \varepsilon_2(1-\Lambda)C\{sis\varphi_2(2c\theta_2 s\nu - s\theta_2 c\nu) + cic\varphi_2\} \\
& \quad - 3Ec\theta_2 s\theta_2 c\varphi_2 + \tfrac{9}{2}Ds\theta_2 c\theta_1 c\varphi_1 = 0
\end{aligned} \tag{4}$$

$$\begin{aligned}
& \tfrac{3}{2}Dc\varphi_1 s\varphi_2 s(\theta_2-\theta_1)\ddot\theta_1 - \tfrac{3}{2}D\{c\varphi_1 c\varphi_2 + s\varphi_1 s\varphi_2 c(\theta_2-\theta_1)\}\ddot\varphi_1 \\
& \quad + E\ddot\varphi_2 - \tfrac{3}{2}Dc\varphi_1 s\varphi_2 c(\theta_2-\theta_1)\left(\dot\theta_1^2 + 2\dot\theta_1 + \dot\varphi_1^2\right) \\
& \quad - 3Ds\varphi_1 s\varphi_2 s(\theta_2-\theta_1)\dot\varphi_1(1+\dot\theta_1) + \tfrac{3}{2}Ds\varphi_1 c\varphi_2\dot\varphi_1^2 \\
& \quad + Es\varphi_2 c\varphi_2\left\{3c^2\theta_2 + (1+\dot\theta_2)^2\right\} - \tfrac{9}{2}Dc\theta_1 c\varphi_1 c\theta_2 s\varphi_2 \\
& \quad - \tfrac{3}{2}Ds\varphi_1 c\varphi_2 - \varepsilon_2 C(1-\Lambda)si(c\theta_2 c\nu + 2s\theta_2 s\nu) = 0
\end{aligned} \tag{5}$$

where the coefficients A, B, C, D, and E are functions of Λ, δ_1, and δ_2 given by

$$A = \Lambda(3+\delta_1+3\delta_2), \qquad B = (1-\Lambda)(2+\delta_2)$$
$$C = (3+\delta_1+\delta_2), \qquad D = -\Lambda(2+\delta_2)$$
$$E = (1-\Lambda)(3+\delta_2)$$

These coefficients represent the influence of the mass distribution of the tether on the system dynamics. It can easily be seen that ε_i is the ratio of the maximum electrodynamic force over bar i to the vertical gravity-gradient force over the system. Equations (2–5) must be integrated from the appropriate initial conditions at $\nu = \nu_0$ to obtain the time evolution of the system.

ProSEDS Tether

ProSEDS is an upcoming flight demonstration of a bare tether system. In ProSEDS a 5-km conductive tether, deployed from an orbiting Delta second stage, is used as the anode of a deboosting system. For stabilization purposes, the conductive wire is connected to a 10-km nonconductive tether with a light end mass attached to it at the other end. Consequently, in ProSEDS-like tethers the second segment is a nonconductive, gravity-gradient stabilizing device; therefore $\varepsilon_2 = 0$, and the equations preceding become simpler.

Tether Conductive over the Whole Length

When the whole tether is conductive, it can be modeled as two identical bars of the same mass and length, leading to

$$m_1 = m_2 = m_T/2, \qquad L_1 = L_2 = L/2, \qquad \Lambda = \tfrac{1}{2}$$
$$2\delta_1 = 2\delta_2 = \delta = m_T/m_B$$

where m_T is the mass of the tether and only one mass distribution parameter remains, δ. Moreover, we will assume that the current is uniform along the tether, that is, $I(s) = I_m$. As a consequence,

$$I_{m_1} = I_{m_2} = I_m, \qquad f_{e_1} = f_{e_2} = \tfrac{1}{2}, \qquad \varepsilon_1 = \varepsilon_2 = \varepsilon$$

In this case Eqs. (2–5) yield

$$\begin{aligned}
&\tfrac{4}{3}[(2\delta+3)/(\delta+4)]c\varphi_1\ddot{\theta}_1 + c\varphi_2 c(\theta_2-\theta_1)\ddot{\theta}_2 - s\varphi_2 s(\theta_2-\theta_1)\ddot{\varphi}_2 \\
&\quad - \tfrac{8}{3}[(2\delta+3)/(\delta+4)]s\varphi_1(1+\dot{\theta}_1)\dot{\varphi}_1 \\
&\quad - 2s\varphi_2 c(\theta_2-\theta_1)\dot{\varphi}_2(1+\dot{\theta}_2) - c\varphi_2 s(\theta_2-\theta_1)\left[\dot{\varphi}_2^2 + (1+\dot{\theta}_2)^2\right] \\
&\quad + \varepsilon\tfrac{4}{3}[(\delta+3)/(\delta+4)]\{ci\{c\varphi_1 + 2c\varphi_2 c(\theta_2-\theta_1)\} \\
&\quad + si(2sv c\theta_1 - cv s\theta_1)(2s\varphi_2 + s\varphi_1)\} + c\varphi_2\{3s\theta_1 c\theta_2 \\
&\quad + s(\theta_2-\theta_1)\} + 4[(2\delta+3)/(\delta+4)]s\theta_1 c\theta_1 c\varphi_1 = 0
\end{aligned} \tag{6}$$

$$\begin{aligned}
&\tfrac{4}{3}[(2\delta+3)/(\delta+4)]\ddot{\varphi}_1 + s\varphi_1 c\varphi_2 s(\theta_2-\theta_1)\ddot{\theta}_2 + \{s\varphi_1 s\varphi_2 c(\theta_2-\theta_1) \\
&\quad + c\varphi_1 c\varphi_2\}\ddot{\varphi}_2 + \{s\varphi_1 c\varphi_2 c(\theta_2-\theta_1) - c\varphi_1 s\varphi_2\}\dot{\varphi}_2^2 \\
&\quad - 2s\varphi_1 s\varphi_2 s(\theta_2-\theta_1)\dot{\varphi}_2(1+\dot{\theta}_2) + \tfrac{4}{3}[(2\delta+3)/(\delta+4)]c\varphi_1 s\varphi_1 \\
&\quad \times \left\{(1+\dot{\theta}_1)^2 + 3c^2\theta_1\right\} + s\varphi_1 c\varphi_2 c(\theta_2-\theta_1)(1+\dot{\theta}_2)^2 \\
&\quad - \varepsilon\tfrac{4}{3}[(\delta+3)/(\delta+4)]\{2sisv\{s\theta_1 + 2s\theta_1 s\varphi_1 s\varphi_2 \\
&\quad + 2s\theta_2 c\varphi_1 c\varphi_2\} + sicv\{c\theta_1 + 2c\theta_1 s\varphi_1 s\varphi_2 + 2c\theta_2 c\varphi_1 c\varphi_2\} \\
&\quad - 2cis\varphi_1 c\varphi_2 s(\theta_2-\theta_1)\} + 3c\theta_1 s\varphi_1 c\theta_2 c\varphi_2 \\
&\quad - s\varphi_1 c\varphi_2 c(\theta_2-\theta_1) + c\varphi_1 s\varphi_2 = 0
\end{aligned} \tag{7}$$

$$\begin{aligned}
&c\varphi_1 c(\theta_2-\theta_1)\ddot{\theta}_1 + s\varphi_1 s(\theta_2-\theta_1)\ddot{\varphi}_1 + \tfrac{2}{3}[(\delta+6)/(\delta+4)]c\varphi_2\ddot{\theta}_2 \\
&\quad + c\varphi_1 s(\theta_2-\theta_1)\dot{\varphi}_1^2 - 2s\varphi_1 c(\theta_2-\theta_1)\dot{\varphi}_1(1+\dot{\theta}_1) \\
&\quad - \tfrac{4}{3}[(\delta+6)/(\delta+4)]s\varphi_2(1+\dot{\theta}_2)\dot{\varphi}_2 + c\varphi_1 s(\theta_2-\theta_1)(1+\dot{\theta}_1)^2 \\
&\quad + \varepsilon\tfrac{4}{3}[(\delta+3)/(\delta+4)]\{cic\varphi_2 + sis\varphi_2(2c\theta_2 sv - s\theta_2 cv)\} \\
&\quad + 2[(\delta+6)/(\delta+4)]s\theta_2 c\theta_2 c\varphi_2 + 3c\varphi_1 c\theta_1 s\theta_2 \\
&\quad - c\varphi_1 s(\theta_2-\theta_1) = 0
\end{aligned} \tag{8}$$

$$\begin{aligned}
&\tfrac{2}{3}[(\delta+6)/(\delta+4)]\ddot{\varphi}_2 - c\varphi_1 s\varphi_2 s(\theta_2-\theta_1)\ddot{\theta}_1 + [c\varphi_1 c\varphi_2 \\
&\quad + s\varphi_1 s\varphi_2 c(\theta_2-\theta_1)]\ddot{\varphi}_1 - [s\varphi_1 c\varphi_2 - c\varphi_1 s\varphi_2 c(\theta_2-\theta_1)]\dot{\varphi}_1^2 \\
&\quad + 2s\varphi_1 s\varphi_2 s(\theta_2-\theta_1)\dot{\varphi}_1(1+\dot{\theta}_1) + c\varphi_1 s\varphi_2 c(\theta_2-\theta_1)(1+\dot{\theta}_1)^2 \\
&\quad + \tfrac{2}{3}[(\delta+6)/(\delta+4)]s\varphi_2 c\varphi_2\left\{(1+\dot{\theta}_2)^2 + 3c^2\theta_2\right\} \\
&\quad + c\varphi_1 s\varphi_2(3c\theta_1 c\theta_2 - c(\theta_2-\theta_1)) + s\varphi_1 c\varphi_2 \\
&\quad - \varepsilon\tfrac{4}{3}[(\delta+3)/(\delta+4)]si\{cvc\theta_2 + 2sv s\theta_2\} = 0
\end{aligned} \tag{9}$$

When $i = 0$, all of the forcing terms are zero except those with $\cos i$. In this case there is an equilibrium position with $\theta_1 = \theta_1(I_m)$, $\theta_2 = \theta_2(I_m)$, and $\varphi_1 = \varphi_2 = 0$, whose stability conditions are analyzed, with a different model, in Refs. 9 and 10. When the current is zero, $\varepsilon_i = 0$, and Eqs. (2–5), or Eqs. (6–9), have a stable equilibrium position along the local vertical, $\theta_1 = \varphi_1 = \theta_2 = \varphi_2 = 0$. In the next section we will analyze the small oscillations of the tether about the local vertical in the case of zero current.

Free Linear Oscillations

The Lagrange equations for $\varepsilon_i = 0$ are linearized about the local vertical, yielding the equations for small oscillations in matrix form:

$$\ddot{\boldsymbol{y}} = M\boldsymbol{y}$$

where

$$\boldsymbol{y} = \begin{Bmatrix} \theta_1 \\ \varphi_1 \\ \theta_2 \\ \varphi_2 \end{Bmatrix}, \qquad M = \frac{1}{K_0}\begin{bmatrix} a_1 & 0 & a_3 & 0 \\ 0 & b_2 & 0 & b_4 \\ c_1 & 0 & c_3 & 0 \\ 0 & d_2 & 0 & d_4 \end{bmatrix}$$

$$K_0 = 12\left\{\delta_1 + \delta_2 + \frac{1}{3}\delta_1\delta_2 + \frac{1}{4}\delta_2^2\right\}$$

$$a_1 = -\frac{6}{\Lambda}\{\delta_2+3\}\{2\delta_1\Lambda + 3(1+\Lambda)\delta_2 + 6\}$$

$$a_3 = \frac{9}{\Lambda}\{(2+\Lambda)\delta_2 + 6\}\{\delta_2 + 2\}$$

$$b_2 = -\frac{1}{\Lambda}\Big\{16\Lambda(\delta_2+3)\delta_1 + 3(7\Lambda+6)\delta_2^2 + 6(11\Lambda+15)\delta_2 + 108\Big\}$$

$$b_4 = \frac{9}{\Lambda}\{(2+\Lambda)\delta_2 + 6\}\{\delta_2 + 2\}$$

$$c_1 = \frac{9}{1-\Lambda}\{\delta_2+2\}\{2\delta_1\Lambda + 3(1+\Lambda)\delta_2 + 6\}$$

$$c_3 = -\frac{6}{1-\Lambda}\{(2+\Lambda)\delta_2 + 6\}\{3\delta_2 + \delta_1 + 3\}$$

$$d_2 = \frac{9}{1-\Lambda}\{\delta_2+2\}\{3(1+\Lambda)\delta_2 + 2\Lambda\delta_1 + 6\}$$

$$d_4 = -\frac{1}{1-\Lambda}\Big\{3(5\Lambda+13)\delta_2^2 + 2(\Lambda+8)\delta_2\delta_1 + 12(4-\Lambda)\delta_1 + 6(\Lambda+26)\delta_2 + 108\Big\}$$

The eigenvalues of the matrix M give the natural frequencies normalized by ω. (Note that the true anomaly v is the independent variable.) They are

$$\sqrt{3}, \qquad \omega_2, \qquad 2, \qquad \omega_4 = \sqrt{1+\omega_2^2}$$

where

$$\omega_2^2 = 3\frac{(6 + 2\delta_2 + \Lambda\delta_2)\,[(3\delta_2 + 2\delta_1)\,\Lambda + 3\delta_2 + 6]}{\Lambda\,(1-\Lambda)\left[3\delta_2^2 + (12 + 4\delta_1)\,\delta_2 + 12\delta_1\right]}$$

The frequencies $\sqrt{3}\omega$ and 2ω correspond to the classical librations of the gravity-gradient pendulum, in-plane and out-of-plane, where the tether moves as a straight bar.[10] The associated eigenvectors are $\{1, 0, 1, 0\}$ and $\{0, 1, 0, 1\}$. The other two correspond to the lateral dynamics of the tether, in-plane ω_2, with eigenvector $\{1, 0, k, 0\}$, and out-of-plane ω_4, with eigenvector $\{0, 1, 0, k\}$. Here k is a negative function of λ, δ_1, and δ_2. Both frequencies have the same qualitative behavior.

The parameter Λ is always in the interval $[0, 1]$, and ω_2 is different from zero for any value of δ_1 and δ_2. Figure 2a shows the dependence of ω_2 on Λ, for arbitrarily chosen values of $\delta_1 = 0.1$ and $\delta_2 = 0.5$. The dependence of ω_4 on Λ is qualitatively identical and quantitatively very similar to ω_2 for $\omega_2 \gg 1$. Note that $\omega_2, \omega_4 \to \infty$ when $\Lambda \to 0$

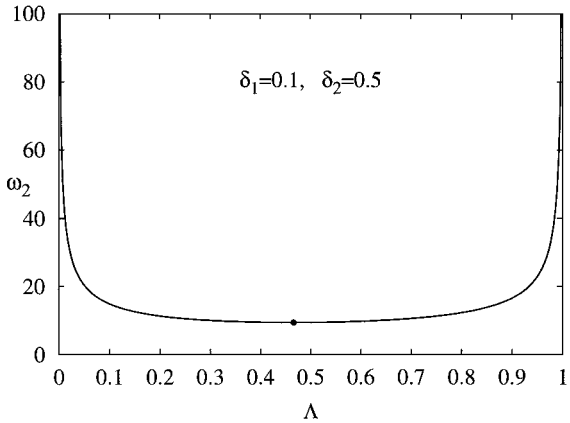

a) Normalized ω_2 vs Λ for $\delta_1 = 0.1$ and $\delta_2 = 0.5$

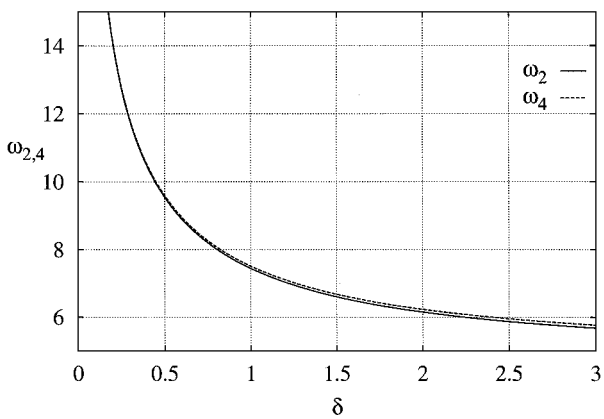

b) Normalized ω_2 and ω_4 vs δ for a fully conductive tether

Fig. 2 Lateral dynamics natural frequencies.

or $\Lambda \to 1$, that is, when one of the two bars disappears. For given values of δ_1 and δ_2, there is a critical value of Λ given by

$$\Lambda^* = \frac{-\delta_2 - 3 + \sqrt{3\delta_2^2 + 12\delta_2 + 9 + \delta_1\delta_2 + 3\delta_1}}{2\delta_2 + \delta_1} \tag{10}$$

where ω_2 and ω_4 reach minimum values. For the particular case in Fig. 2a, we have $\Lambda^* \simeq 0.466$. The minimum values of the frequencies are $\omega_2^* \simeq 9.42$ and $\omega_4^* \simeq 9.47$. This qualitative behavior does not change within the range of interest for the parameters δ_1 and δ_2. Thus, ω_2 never vanishes and grows to infinity in the limits $\Lambda \to 0$ and $\Lambda \to 1$.

As an example of a nonuniform tether, we consider the ProSEDS tether. The ProSEDS tether is composed of $L_1 = 5$ km of conductive wire with an overall linear density of $\rho_1 \simeq 2$ kg/km and $L_2 = 10$ km of nonconductive tether with a linear density of $\rho_2 \simeq 0.2$ kg/km. The overall length is $L = L_1 + L_2 = 15$ km, and the mass attached to its free end is $m_B = 20.4$ kg. For this tether $\Lambda = \frac{1}{3}$, $\delta_1 \simeq 0.49$, and $\delta_2 \simeq 0.098$, and the frequencies associated to the lateral dynamics are

$$\omega_2 \simeq 8.81, \qquad \omega_4 \simeq 8.87$$

In this case, the minimum values of frequencies would be $\omega_2^* \simeq 8.437$ and $\omega_4^* \simeq 8.496$ for $\Lambda^* \simeq 0.475$.

For a uniform electrodynamic tether, which is conductive over the whole length, we have

$$\omega_2 = \sqrt{\frac{3(5\delta + 24)(11\delta + 24)}{\delta(7\delta + 48)}}, \qquad \omega_4 = \sqrt{1 + \omega_2^2}$$

where $\delta = m_T/m_B$. The two normalized frequencies are shown in Fig. 2b as a function of δ.

Note that ω_2 and $\omega_4 \to \infty$ when $\delta \to 0$. This reflects the typical behavior of a massive system in which at least one natural frequency increases as the mass decreases. The two frequencies ω_2 and ω_4 are never equal, but they are very close over a large range of δ values.

Nonlinear Stability Analysis

In this section, we analyze certain aspects of the dynamic stability properties of the system, following the procedure used in Ref. 8. In Ref. 8, we showed that the linear stability analysis was not conclusive, and we had to carry out a nonlinear analysis to clarify the behavior of the perturbed system. Consequently, here we directly attack the nonlinear analysis.

The two cases studied in this paper exhibit the same qualitative behavior. When no current is flowing in the wire, the parameters ε_i in Eqs. (2–5) are equal to zero, and the system has a stable equilibrium position along the local vertical, $\theta_1 = \varphi_1 = \theta_2 = \varphi_2 = 0$. However, this steady solution disappears when a nonzero current is flowing in the wire ($\varepsilon_i \neq 0$), and a periodic solution (a closed orbit in phase space) takes the place of the equilibrium position. For small values of ε_i, a perturbation method can be used to compute this periodic solution, as shown in Ref. 8.

However, there are some similarities and differences with that analysis that must be pointed out. As in Ref. 8, the forcing terms associated with the electrodynamic forces are periodic, and because of the simplified model adopted, their period is the orbital period. In Ref. 8, the only source of parametric resonance in the system was the frequency 2ω associated with the out-of-plane motion. In the present dynamic model, there are two additional sources of possible resonances: For certain values of the parameters Λ, δ_1, and δ_2, the natural frequencies ω_2 or ω_4 may become multiples of the orbital frequency. Fortunately, these multiples are not small (typically greater than 7), and the resonances associated with these cases are not as strong as the resonance associated with the natural frequency 2ω. Therefore, in this paper we limit our analysis to the cases in which the natural frequencies ω_2 and ω_4 take nonresonant values. We look for the periodic solution that, when $\varepsilon_i \neq 0$, replaces the steady equilibrium position at zero current.

The stability properties of this periodic orbit are studied with the same method used in Ref. 8. An approximate periodic solution of Eqs. (2–5), $\boldsymbol{y}_p(\nu, \varepsilon_1, \varepsilon_2, \Lambda, \delta_1, \delta_2, i)$ is found through a perturbation method in powers of the small parameters ε_i. This solution is perturbed: $\boldsymbol{y} = \boldsymbol{y}_p + \boldsymbol{\eta}(\nu, \varepsilon_1, \varepsilon_2, \Lambda, \delta_1, \delta_2, i)$. Equations (2–5) are linearized about the periodic solution $\boldsymbol{y}_p$, leading to linear equations in $\boldsymbol{\eta}$, which are the variational equations of the system as follows:

$$\dot{\boldsymbol{\eta}} = \mathcal{J}(\boldsymbol{y}_p, \nu, \varepsilon_1, \varepsilon_2, \Lambda, \delta_1, \delta_2, i) \cdot \boldsymbol{\eta} \tag{11}$$

where $\mathcal{J}$ is the Jacobian matrix of the governing equations computed for the periodic solution $\boldsymbol{y}_p$. Equations (11) are linear equations with 2π-periodic variable coefficients, and the stability of its solutions can be analyzed by means of Floquet theory (see Ref. 13). The stability properties of the periodic solution $\boldsymbol{y}_p$ depend on its monodromy matrix $M(\varepsilon_1, \varepsilon_2, \delta_1, \delta_2, i)$, which is now an 8×8 matrix. However, obtaining M and its eigenvalues through an asymptotic expansion in powers of ε_i, as was done in Ref. 8 with a 4×4 matrix, is no longer possible due to the size of M. This matrix must be computed numerically for each particular case under study.

Analysis of ProSEDS-Type Tethers

For ProSEDS-type tethers (Fig. 3), Eqs. (2–5) of this model take a simpler form because $\varepsilon_2 = 0$ and A, B, C, D, and E take fixed numerical values. When the values of the ProSEDS tether stated earlier are used, the periodic solution we find in this case, to order ε_1^4, is

$$\theta_1 = \{-11867ci\varepsilon_1 + 996.8s^2 i \sin 2\nu\varepsilon_1^2 + [(371.8\cos 2\nu + 276.8)s^2 i - 5.92c^2 i]ci\varepsilon_1^3 + [(-9.381s^2 i - 50.64c^2 i)\sin 2\nu + 26.05s^2 i \sin 4\nu]s^2 i\varepsilon_1^4 + \mathcal{O}(\varepsilon_1^5)\} \cdot 10^{-5} \tag{12}$$

$$\varphi_1 = \{11867si\cos\nu\,\varepsilon_1 - 2816cisi\sin\nu\varepsilon_1^2 + [(20.0s^2i + 31.38c^2i)\cos\nu - 123.1s^2i\cos 3\nu]si\varepsilon_1^3 + [(19.83s^2i - 34.73c^2i)\sin\nu + 54.2s^2i\sin 3\nu]cisi\varepsilon_1^4 + \mathcal{O}(\varepsilon_1^5)\}\cdot 10^{-5} \tag{13}$$

$$\theta_2 = \{25.0s^2i\sin 2\nu\varepsilon_1^2 + 4.97cis^2i\cos 2\nu\varepsilon_1^3 + [(1126c^2i + 964.1s^2i)\sin 2\nu - 19872s^2i\sin 4\nu]\cdot 10^{-3}s^2i\varepsilon_1^4 + \mathcal{O}(\varepsilon_1^5)\}\cdot 10^{-3} \tag{14}$$

$$\varphi_2 = \{1.521s^3i\cos 3\nu\varepsilon_1^3 - 0.6915cis^3i\sin 3\nu\varepsilon_1^4 + \mathcal{O}(\varepsilon_1^5)\}\cdot 10^{-3} \tag{15}$$

The solution used in the numerical computations has been obtained to order five, although only four terms are shown here for the sake of brevity. Figure 4a shows this solution for different values of orbital inclination, and Fig. 4b shows the influence of electric current through ε_1. Only positive values of ε_1, causing drag on the tether, have been considered here, but the periodic solution is also valid for $\varepsilon_1 < 0$, propulsive tether. (In that case, θ_1 would be positive.) Note that the in-plane angle θ_1 is almost constant, decreasing with inclination and increasing with the strength of the electrodynamic force, θ_2 and φ_1 increase with both, and φ_2 is very small.

In this case, the monodromy matrix M of the variational equations (11) only depends on ε_1 and i, the other parameters being fixed. In general, its characteristic polynomial has four pairs of conjugate complex roots.

Figure 5a shows the moduli of the eigenvalues, as a function of the parameter ε_1 for different values of the inclination in the (high) range 30–75 deg. Because the numerical accuracy of the asymptotic solution increases as $i \to 0$, the curves have been computed for different ranges of ϵ_1 to keep a constant accuracy. All eigenvalues come in pairs of complex conjugates, so that only four curves appear for each inclination. Two pairs always have $|\lambda| > 1$ (unstable eigenvalues), and the other two have $|\lambda| < 1$ (stable eigenvalues). Note that the moduli of one stable and one unstable pair have a very small sensitivity to variations of i and remain always very close to unity.

The other two pairs, however, show a high sensitivity to changes of the orbital inclination i and the parameter ε_1. In fact, for values of ε_1 above a critical value, these roots grow quickly and they are the main source of instability for the system. Figure 5b shows the moduli of the eigenvalues for (low) values of $i = 7.5$–20 deg. The rapid growth of the eigenvalue for ε_1 greater than a critical value is apparent. The eigenvalue reaches a maximum, and after that, it decreases. This behavior is not seen in the higher inclinations because the range of ϵ_1 that can be attained is smaller.

The different behavior of the two sets of eigenvalues is an important point of this analysis with respect to Ref. 8. We will carry out a detailed study to show more clearly the differences. In Ref. 8, the eigenvalues of the 4×4 monodromy matrix for a rigid tether are obtained as an asymptotic expansion in powers of a small parameter ε, which is equivalent to $si\varepsilon_1$. The moduli of the eigenvalues were

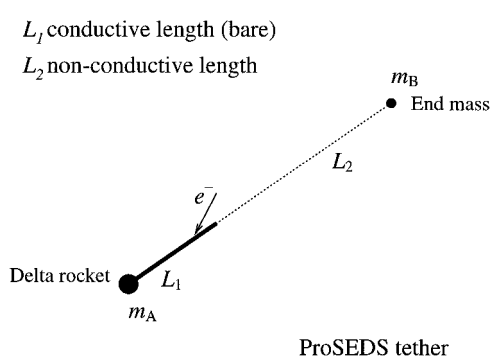

Fig. 3 ProSEDS configuration.

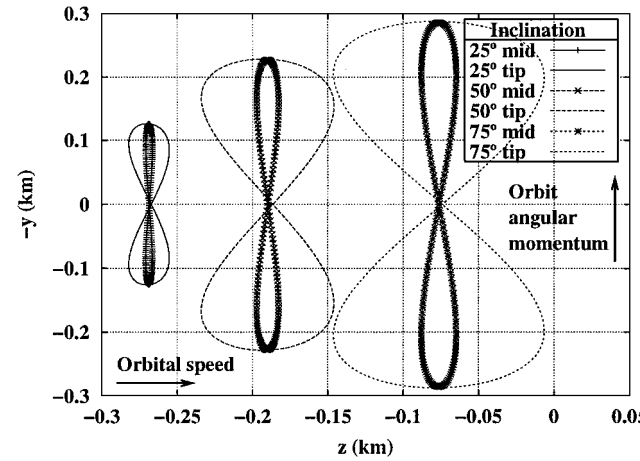

a)

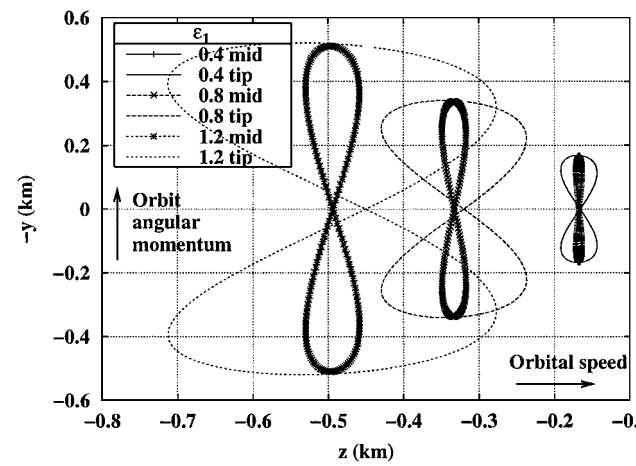

b)

Fig. 4 Periodic solution for a ProSEDS-type tether (projection of the midpoint and tip trajectories on the local horizontal plane) as a function of a) orbital inclination ($\varepsilon_1 = 0.5$) and b) electric current ($i = 45$ deg).

given by

$$|\lambda_{1,2}| = 1 + (\pi/9)cis^2i\,\varepsilon_1^3 + \mathcal{O}(\varepsilon_1^4)$$

$$|\lambda_{3,4}| = 1 - (\pi/9)cis^2i\,\varepsilon_1^3 + \mathcal{O}(\varepsilon_1^4)$$

In the present case, there are four pairs of complex-conjugate numbers. Two pairs have a behavior very similar to that exhibited by the eigenvalues just given. The best way to see this similarity is to plot $\sigma = (|\lambda| - 1)/\varepsilon_1^3$ vs ε_1.

Note that σ stays constant, to order ε^3, for the eigenvalues obtained in Ref. 8. Consequently, any eigenvalue with a similar behavior must have an associated σ that stays constant, in a first approximation, as a function of ε_1.

Figures 6 show the numerically computed values of σ vs ε_1. There are two pairs (four eigenvalues) for which the value of σ is almost constant, as shown in Fig. 6a. The remaining eigenvalues have a rather different behavior, as shown in Fig. 6b. Note the very different scale of the ordinate axes of Figs. 6. The values of i are the same as in Fig. 5b, and the lower value in Fig. 5a, 7.5–30 deg.

These computations were carried out for $\varepsilon_1 \sin i \in [-0.6, 0.6]$, which ensures similar numerical accuracy, because the asymptotic expansions are more accurate for small i.

The eigenvalues in Fig. 6a correspond to the vibration modes in which the tether moves as a rigid bar. They are a source of instability for the system, but they do not involve any new effects when compared to the analysis carried out in Ref. 8 for the rigid tether.

The eigenvalues in Fig. 6b correspond to the first lateral mode of the tether both in-plane and out-of-plane. They reflect the influence of the tether lateral dynamics on the system's response to

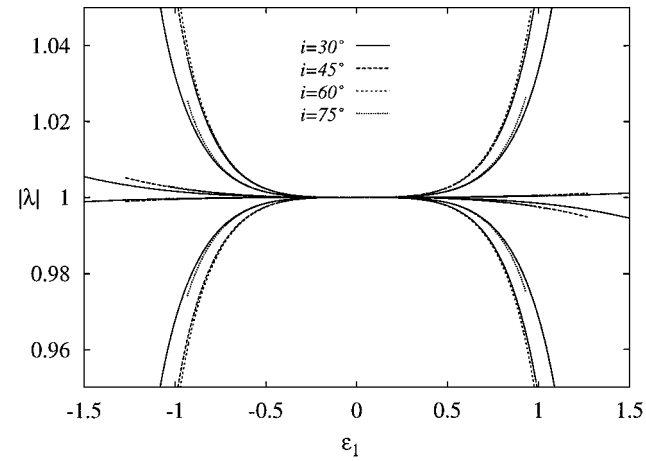

a) High inclination

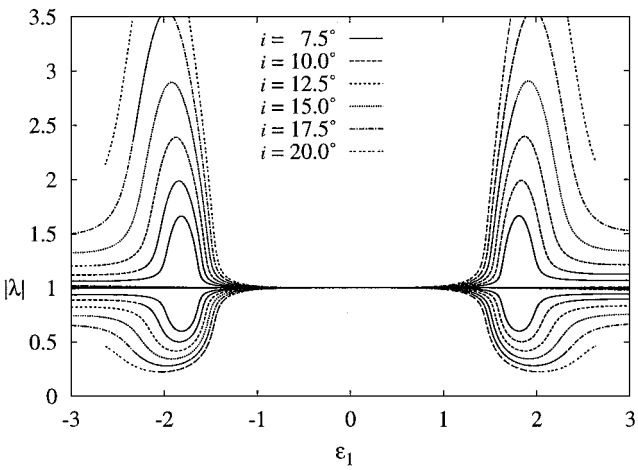

b) Low inclination

Fig. 5 Moduli of the monodromy matrix eigenvalues for a ProSEDS-type tether.

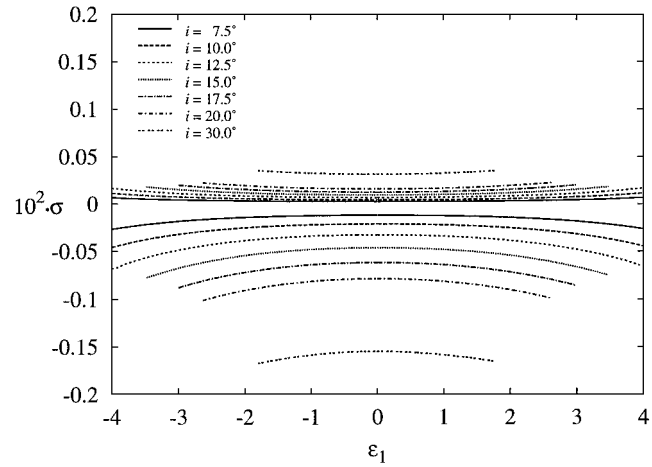

a) σ for $\lambda_{1,2}$, $\lambda_{3,4}$

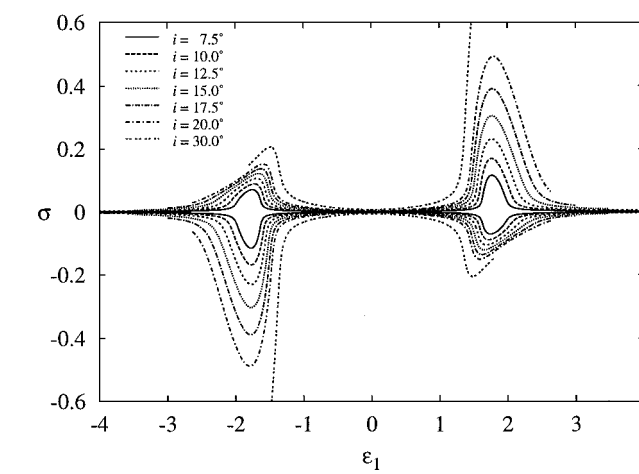

b) σ for $\lambda_{5,6}$, $\lambda_{7,8}$

Fig. 6 Third-order coefficient σ of the monodromy matrix eigenvalues for a ProSEDS-like tether vs ϵ_1 and different values of *i*.

electrodynamic forces. They show a new behavior characterized by a much greater sensitivity to the electrodynamic excitation. It is clear now that they are the main source of instability for this kind of tether. This analysis shows that the tether lateral dynamics has a negative influence on the stability properties of the system. In fact, the lateral dynamic of the tether makes the destabilizing mechanism of electrodynamic tethers more sensitive to the orbital inclination.

In summary, for all values of ε_1 and i, there are four unstable eigenvalues with moduli greater than unity. This means that the periodic solution is always unstable, within the limits of this model, and as a consequence, any small perturbation causes the motion to depart from the periodic solution. Thus, after a while the dynamics results in net flux of energy of electrodynamic origin into the system. This conclusion, of course, is valid within the simplified assumptions of our model in which damping, variation of the tether current along the orbit, and other excitation frequencies have been neglected. As a matter of fact, numerical simulations with accurate dynamic and environmental models do show the insurgence of a strong lateral (skip-rope) motion.[1,2] However, in many cases, the skip rope is not strong enough to destabilize the whole system because energy is dissipated by the tether material damping through nonlinear coupling with the tether stretching modes.

Our numerical calculation process has a clear restriction: The periodic solution needed to integrate the variational equations (11) is obtained through an asymptotic expansion (12–15) valid only for small values of ε_1. To expand the validity range, the solution has been computed up to order 5. Thus, terms of order ε_1^6 that give errors of 5% for $\varepsilon_1 \sin i = 0.6$ have been neglected. Therefore, in our analysis we restrict the interval of variation of $\varepsilon_1 \sin i$ to $[-0.6, 0.6]$. However, the intrinsic instability of the system (without damping) should remain for values of ε_1 of order unity because no new physical effects appear when ε_1 grows.

Tether Conductive over the Whole Length

When the whole tether is conductive, there are three free parameters: i, ε, and $\delta = m_T/m_B$, which was fixed for the ProSEDS-type tether cases. This new degree of freedom allows some insight on whether the tether mass can be optimized for stability. The evolution of the eigenvalues with δ, in fact, shows the influence of the tether mass distribution on the stability of the system. Again, an approximate periodic solution is derived up to order 5 with the help of MapleV. The first three terms are

$$\theta_1(\nu) = -\varepsilon \cdot 4\frac{\delta+3}{11\delta+24}ci + \varepsilon^2 \cdot A_0 \sin 2\nu + \varepsilon^3 \cdot (A_1 + A_2 \cos 2\nu) + \mathcal{O}(\varepsilon^4) \tag{16}$$

$$\varphi_1(\nu) = +\varepsilon \cdot 4\frac{\delta+3}{11\delta+24}si\cos\nu + \varepsilon^2 \cdot B_0 \sin\nu + \varepsilon^3 \cdot (B_1 \cos\nu + B_2 \cos 3\nu) + \mathcal{O}(\varepsilon^4) \tag{17}$$

$$\theta_2(\nu) = -\varepsilon \cdot \frac{4}{3}\frac{\delta+3}{5\delta+24}ci + \varepsilon^2 \cdot C_0 \sin 2\nu + \varepsilon^3 \cdot (C_1 + C_2 \cos 2\nu) + \mathcal{O}(\varepsilon^4) \tag{18}$$

$$\varphi_2(\nu) = +\varepsilon \cdot \frac{4}{3}\frac{\delta+3}{5\delta+24}si\cos\nu + \varepsilon^2 \cdot D_0 \sin\nu + \varepsilon^3 \cdot (D_1 \cos\nu + D_2 \cos 3\nu) + \mathcal{O}(\varepsilon^4) \tag{19}$$

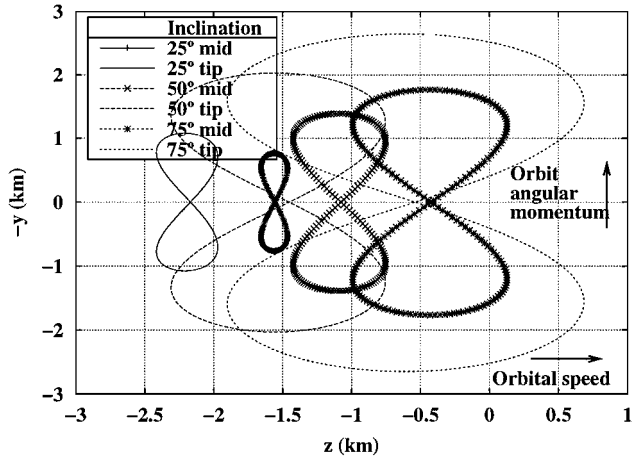

a)

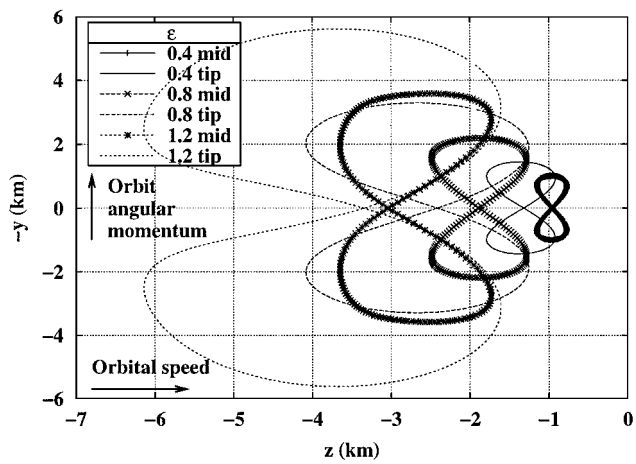

b)

Fig. 7 Periodic solution for a fully conductive tether (projection of the midpoint and tip trajectories on the local horizontal plane) vs a) orbital inclination ($\varepsilon = 0.5$) and b) current intensity parameter ϵ ($i = 45$ deg).

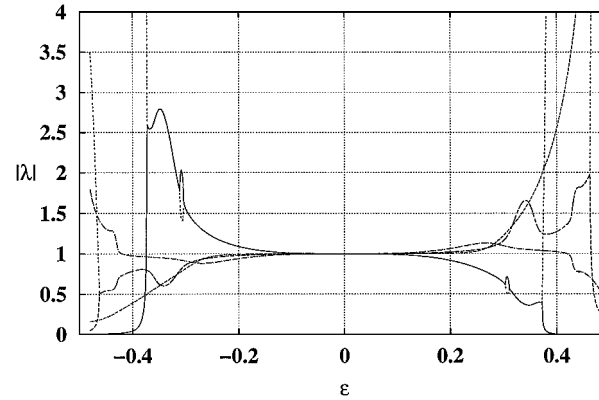

a) $\delta = 1.50$ and $i = 12$ deg

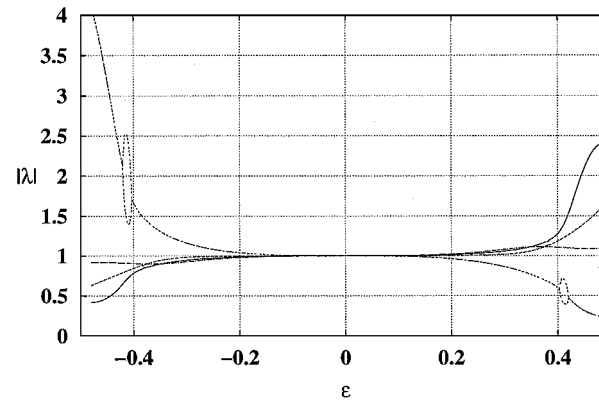

b) $\delta = 1.50$ and $i = 16$ deg

Fig. 8 Moduli of the monodromy matrix eigenvalues vs ε for two cases showing a specially complex dynamics.

where the coefficients A_0–D_2, which are functions of i and δ, may be found in the Appendix. The terms of order 4 and 5 are too complex to be written in full.

Figure 7a shows the periodic orbit for different values of the inclination and a constant ε, and Fig. 7b shows the trajectories for constant inclination and different ε. In both cases, arbitrary values $\delta = 1$ and $L_1 = L_2 = 7.5$ km have been chosen to keep similarity with the earlier cases. The curves show the projection of the tether midpoint and tip on the local horizontal plane. There is a similarity with the plots of ProSEDS (Fig. 4). The curves have the same qualitative behavior, but the deviations are much greater and φ_2 is no longer small. This is expected because the conducting wire is three times as long, and the electrodynamic torque is much stronger than in the ProSEDS cases for the same value of tether current.

The variational equations (11) about the new solution (16–19) are derived, and the eigenvalues of the monodromy matrix M are computed numerically. Now, the eigenvalues depend on the parameter δ as well. This allows for a much richer dynamics.

As δ and i increase, the eigenvalues of M are no longer four pairs of complex conjugates, but some of them bifurcate into two real numbers, joining again for higher values of ϵ. This happens mostly at high currents, but in some ranges, heavy tethers with $\delta > 1.2$ and $i \in [10, 20 \text{ deg}]$ bifurcations also occur at low current intensity and inclination. Two such cases are shown in Fig. 8. The eigenvalues keep the same general shape as in the ProSEDS case, with severe bifurcations superimposed. This is repeated several times as ε grows, with new and stronger bifurcations opening and closing, but the limited range of the approximate solution does not allow for further exploration. To some extent, the strong bifurcations mask the "humps" of the lateral eigenvalues.

For lighter tethers, the dynamics is more similar to that of the ProSEDS-like tethers in which two groups of eigenvalues can be distinguished. In spite of the difficulty of associating the eigenvalues of the monodromy matrix with those of the free oscillations of the system, comparison with the ProSEDS cases and with the analysis in Ref. 8 allows for a safe correlation.

Figure 9 shows the evolution of σ vs ϵ, for a fixed inclination and different mass distributions. The eigenvalues can be clearly divided into two groups: those associated to lateral motion (Fig. 9a) and those corresponding to rigid-body motion (Fig. 9b).

In the first group, there is a maximum value of σ for each case, reaching a peak for a moderate value of δ. As expected, maxima occur at higher currents as δ grows: Heavier tethers are more stable. These maxima, as those in the ProSEDS case, are very interesting. The gaps close to the zero of ε in Fig. 9 and in Fig. 10 are due to loss of numerical precision because $\sigma \to 0/0$ as $\varepsilon \to 0$.

The lateral motion eigenvalues cross several times; this can be seen in Figs. 8 and 10 as well. One, between the maxima, is clear. Other very quick crossings occur beyond the maxima and are nearly masked by the step size in ϵ. Note that, for a specific system, one should avoid the value of ϵ corresponding to maximum instability.

A wide exploration of parameters shows that maxima increase in magnitude and occur at lower values of current as δ decreases, which is consistent with the behavior of a very light tether, that is, very small transverse forces cause large deviations. As far as the lateral motion is concerned, heavy tethers (relative to the end mass) are more stable, or rather less unstable, at low current intensities (below the value corresponding to the maxima) and light tethers are slightly more stable at high intensities. In all cases, the first crossing is the less unstable spot.

Rigid-body motion, as in the ProSEDS case, shows little variation with current intensity, except at high values of ϵ, where instability suddenly increases. This is also consistent with the constant term in the rigid-bar analysis of Ref. 8. The eigenvalues are much larger, as expected because the whole length is conductive instead of the

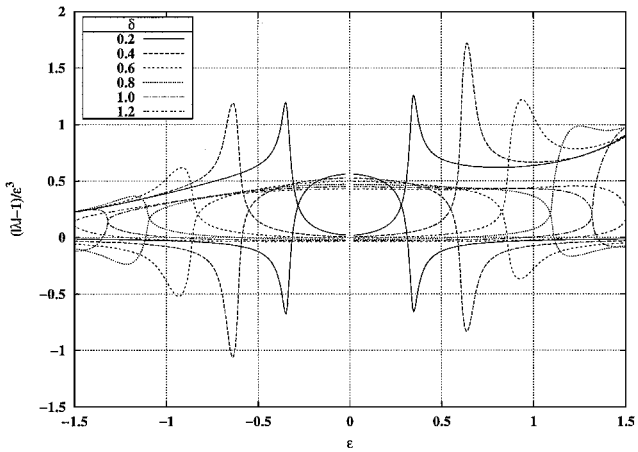

a) Lateral motion vs tether mass, $i = 10$ deg

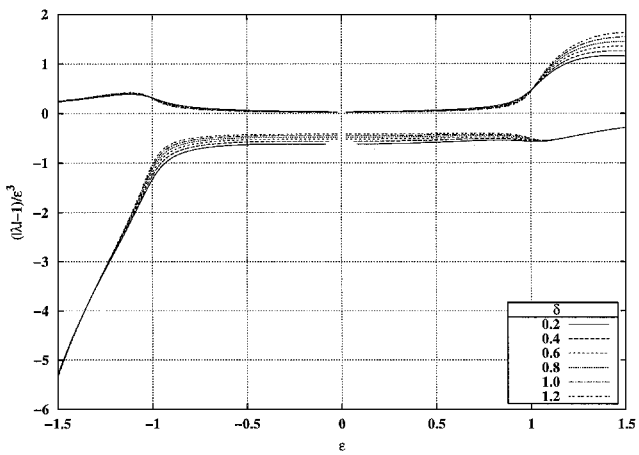

b) Rigid-body motion vs tether mass, $i = 10$ deg

Fig. 9 Effect of tether mass distribution $\delta = m_T/m_B$ for low inclination.

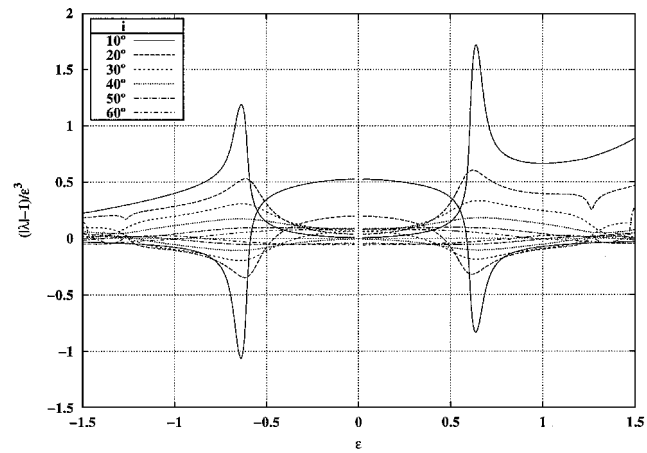

a) Lateral motion

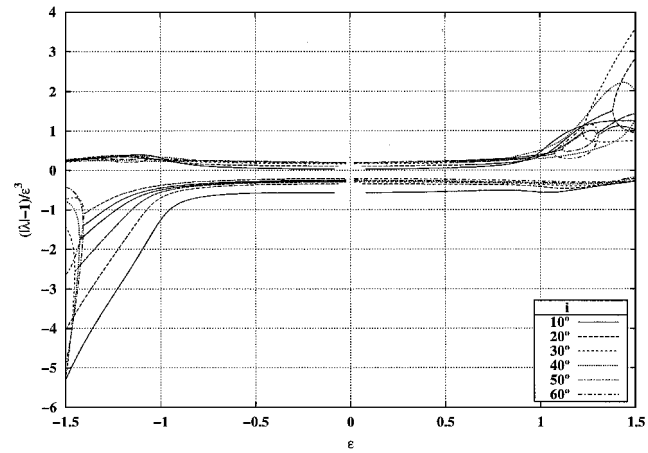

b) Rigid-body motion

Fig. 10 Effect of inclination for a light tether, $\delta = 0.4$.

inner third and torque is nine times greater for the same current intensity.

Figure 10 shows the behavior of a light tether ($\delta = 0.4$) with orbital inclination. The same maxima and crossings can be appreciated. The behavior is similar to the ProSEDS case, with maxima for each curve, although much more unstable due to the higher electrodynamic torque, especially in the rigid-body motion. This can also be seen in Fig. 8, where the behavior for small current intensities is similar to that of Pro-SEDS, but later becomes blurred by the bifurcations.

In the rigid-body motion, σ is nearly constant with ϵ for moderate currents. For higher currents, it increases sharply and shows a complex behavior with recurring bifurcations. However, our analysis loses accuracy for higher ϵ due to the power expansion periodic solution.

Note that the maxima increase in magnitude as the inclination decreases, but occur at higher current intensities, that is, a sizable out-of-plane forcing term is needed for instability at low inclinations. Moreover, a higher inclination means a weaker instability for the lateral dynamics, both at low and at high current intensities.

Summary of Results

We have derived a model that explains the main features of the dynamics of an electrodynamic tether by taking into account the tether lateral dynamics in a simplified manner, that is, the tether is modeled as two rigid bars articulated at their common end. In this way, the lateral dynamics of tethers made of a single wire or of conductive and nonconductive portions can be approximately described. When the current flowing in the conductive portion of the tether is zero, the system has a stable equilibrium position with the tether along the local vertical. This steady solution disappears when the current in the wire is not zero. After the assumption that the current in the tether is constant, an ω-periodic solution takes the place of the steady equilibrium position in the state space. Because of our simplified environmental model, the period of the periodic solution is the orbital period. In a more general case, however, the solution will contain multiples of the orbital frequency.

The stability properties of this periodic solution have been obtained by analyzing the variational equations that describe the behavior of any perturbation superimposed on the periodic orbit. These equations are linear, with ω-periodic coefficients. Their long-term behavior has been investigated, with the help of the Floquet theory.

Our analysis focused on two particular cases: 1) a tether with a conductive section and an inert section and 2) a tether conductive over the whole length. In both cases, we obtained the eigenvalues of the monodromy matrix as a function of the free parameters: the average current in the wire, the orbital inclination, and, in the second case, also the system mass ratio m_T/m_B. The main conclusions are as follows.

ProSEDS-Type Tether

The eight eigenvalues of the monodromy matrix are four pairs of complex-conjugate numbers. Half of them have moduli greater than unity for any orbital inclination above zero. Consequently, the periodic solution is always unstable, which, within the limits of this model, means that there is a net energy flux of electrodynamic origin into the system.

The behavior of two pairs of eigenvalues is similar to that shown in Ref. 8, where the system was modeled as one bar. For a given orbital inclination, and for small tether currents, the differences of the eigenvalue moduli from unity depend on the third power of the current, that is, this instability is weak.

The moduli of the other two pairs of eigenvalues, which are associated with the lateral dynamics, exhibit a different behavior. For any orbital inclination (which must be different from zero in this model),

they show a rapid growth for a tether current above a critical value. These eigenvalues are the most important source of instability for the system. The lateral dynamics of the tether makes the destabilizing mechanism more sensitive to the orbital inclination.

These instabilities apply to an electrodynamic tether operating in either the thrust (boost) or generator (deboost) mode. One of the main dynamic effects of the instability is the development of a large skip rope motion of the tether, that is, the combined excitation of the first lateral mode both in-plane and out-of-plane. The instability mechanism presented in this paper provides a description of the origin, onset, and development of the skip-rope motion that has been observed in detailed numerical simulations.

Tether Conductive over the Whole Length

Similar conclusions can be obtained for the fully conductive tether, with some distinctive points:

1) The dynamics is richer, as a consequence of the higher number of free parameters, showing regions of successive bifurcations.

2) The rigid-body instability, though qualitatively similar, is stronger than in ProSEDS-type tethers of comparable lengths and current intensity due to the higher forcing torque.

3) For fixed values of the pair (i, δ), instability peaks at a specific current intensity ε. If inclination and current intensity are mission determined, an appropriate choice of the mass ratio δ can lead to a smaller instability region and less need for control.

This analysis deliberately uses a simplified model to capture the essential mechanism of the instability. Obviously, the dynamic simulation of a specific tethered system should take into account other effects such as damping, plasma density influence on electric current, elasticity, orbital eccentricity, and a control system. However, including them would result in much more complex equations, and it would be difficult to trace the contribution of each one.

Damping, for example, internal dissipation in the tether, has not been considered, although it would obviously have a stabilizing effect by taking mechanical energy out of the system. The authors have studied the effect of damping in the simpler, one-bar model of Ref. 8, finding some regions in parameter space where motion is stable.[14] This work still has to be extended to the present two-bar model.

Elasticity causes an instability of its own, as was mentioned earlier.[10] A rigid, articulated model has been chosen, among other things, to show that this new instability is independent of elasticity. In Ref. 15, the authors have used different models, elastic and inextensible, finding little difference in the growth of instability.

Electric current has been assumed constant in time. Actually, it depends on plasma density, which is maximum in the poles. Therefore, current changes with twice the orbital frequency, in resonance with the out-of-plane oscillations. Corsi and Iess studied this resonance for a dumbbell system and found that it plays a major destabilizing role, but that it can be controlled.[16] The authors have studied the same resonance with a model that takes into account the lateral dynamics, and it certainly grows faster, but not as much as in the dumbbell model. Besides, both can be cotrolled with simple, energy-related control laws.[15]

For a bare tether operating in the deboost regime, some results about the stability problem including the variation of tether current along the orbit may be found in Ref. 17, where a rigid-bar model is used for the tether.

Conclusions

A relatively simple model of two articulated tether bars leads to key insights into the dynamics of a tether system driven by electrodynamic forces. This model is a further evolution of the dumbbell tether model (a single straight bar) that has been utilized repeatedly by many authors to study the dynamics of tether systems and recently by these authors to study the librational instability of electrodynamic tethers. The stability analysis carried out by means of the two-bar model shows that the two modes of oscillation (the tether libration and the lateral oscillation) are both unstable in the absence of damping. The model confirms that the librational instability (as reported in previous work) grows very slowly while the lateral oscillation instability grows at a faster rate. The lateral oscillation instability depends on the tether mass over the satellite mass ratio, the orbital inclination, and the ratio between the maximum lateral electrodynamic force and the vertical gravity-gradient force. In brief, the lateral instability increases with the increase of the orbital inclination. The instability shows a rapid rate of growth above a critical value of the electrodynamic to gravity-gradient force ratio. With regards to the tether-to-satellite mass ratio, heavy tethers are less unstable at low current intensities, and light tethers are less unstable at higher current intensities. Finally, ballasted electrodynamic tether configurations (in which a nonconductive tether portion is added to increase the gravity-gradient torque) reduce the rate of growth of the librational instability because of the reduced strength of the electrodynamic torque when compared with an all-conductive tether for an equal value of the current.

Appendix: Coefficients of the Periodic Solution

$$A_0 = \frac{64}{3}\frac{(1511\delta^3 + 13872\delta^2 + 41760\delta + 41472)(\delta+3)^2}{(5\delta+24)(11\delta+24)^2(137\delta^2+960\delta+1728)}\,s^2 i, \qquad B_0 = -\frac{32}{9}\frac{(37\delta+120)(\delta+3)^2}{(5\delta+24)(11\delta+24)^2}\,cisi$$

$$C_0 = \frac{64}{9}\frac{(2317\delta^3 + 29400\delta^2 + 122400\delta + 165888)(\delta+3)^2}{(5\delta+24)^2(11\delta+24)(137\delta^2+960\delta+1728)}\,s^2 i, \qquad D_0 = -\frac{32}{9}\frac{(\delta+3)^2}{(5\delta+24)^2}\,cisi$$

$$A_1 = -\frac{32}{27}\frac{cis^2 i(\delta+3)^3}{(5\delta+24)^2(11\delta+24)^4}\{(8612\cot^2 i - 12007)\delta^3 - (79272 - 88992\cot^2 i)\delta^2$$
$$-(179712 - 266112\cot^2 i)\delta + 221184\cot^2 i - 152064\}$$

$$A_2 = \frac{32}{9}\frac{cis^2 i(\delta+3)^3(2227927\delta^5 + 39149688\delta^4 + 271889856\delta^3 + 933064704\delta^2 + 1581907968\delta + 1059028992)}{(137\delta^2+960\delta+1728)(5\delta+24)^3(11\delta+24)^3}$$

$$B_1 = \frac{32}{27}\frac{s^3 i(\delta+3)^3}{(137\delta^2+960\delta+1728)(5\delta+24)^2(11\delta+24)^4}\{(3536950 + 840769\cot^2 i)\delta^5 + (14088504\cot^2 i + 61305888)\delta^4$$
$$+(409167072 + 89586432\cot^2 i)\delta^3 + (267604992\cot^2 i + 1309754880)\delta^2$$
$$+(364621824\cot^2 i + 2005420032)\delta + 167215104\cot^2 i + 1170505728\}$$

$$B_2 = \frac{64}{15}\frac{s^3 i(\delta+3)^3}{(109\delta^2+768\delta+1728)(137\delta^2+960\delta+1728)(5\delta+24)^3(11\delta+24)^3}(62302171\delta^7 + 1436038464\delta^6 + 13860763824\delta^5$$
$$+72461809152\delta^4 + 221103820800\delta^3 + 392932933632\delta^2 + 375819927552\delta + 149060321280)$$

$$C_1 = -\frac{32}{81}\frac{cis^2 i(\delta+3)^3}{(11\delta+24)^2(5\delta+24)^4}\{(3356\cot^2 i - 4977)\delta^3 + (40608\cot^2 i - 40680)\delta^2$$
$$+ (162432\cot^2 i - 89856)\delta + 221184\cot^2 i - 41472\}$$

$$C_2 = \frac{32}{27}\frac{cis^2 i(\delta+3)^3(6545537\delta^5 + 112897464\delta^4 + 760497984\delta^3 + 2494844928\delta^2 + 3979984896\delta + 2460450816)}{(137\delta^2+960\delta+1728)(5\delta+24)^3(11\delta+24)^3}$$

$$D_1 = \frac{32}{27}\frac{s^3 i(\delta+3)^3}{(137\delta^2+960\delta+1728)(11\delta+24)^2(5\delta+24)^4}\{(541798+125629\cot^2 i)\delta^5 + (2481576\cot^2 i + 10882848)\delta^4$$
$$+ (19512576\cot^2 i + 85685472)\delta^3 + (329937408 + 76667904\cot^2 i)\delta^2$$
$$+ (619923456 + 150958080\cot^2 i)\delta + 119439360\cot^2 i + 453869568\}$$

$$D_2 = \frac{64}{405}\frac{s^3 i(\delta+3)^3}{(109\delta^2+768\delta+1728)(137\delta^2+960\delta+1728)(5\delta+24)^3(11\delta+24)^3}\{30398722257\delta^7 + 845149577288\delta^6 + 9891479947688\delta^5$$
$$+ 63091462947840\delta^4 + 236496219955208\delta^3 + 520231549501440\delta^2 + 621233254563840\delta + 310618777190400\}$$

Acknowledgments

The work of the first three authors has been carried out with the support of the Spanish Agency Dirección General de Educación Superior e Investigación Científica under Grant PB97-0574-C04-04. The contribution of E. C. Lorenzini was supported by Grant NAS8-1605 from NASA Marshall Space Flight Center.

References

[1]Lorenzini, E., Estes, R., Cosmo, M., Forward, R., Sanmartín, J., Peláez, J., and Kaiser, M., "In-Space Transportation with Tethers," NASA Final Rept., Grant NAG8-1303, Harvard–Smithsonian Center for Astrophysics, Sept. 1999.

[2]Lorenzini, E., Estes, R., Cosmo, M., and Peláez, J., "Dynamical, Electrical and Thermal Coupling in a New Class of Electrodynamic Tethered Satellites," *Spaceflight Mechanics 1999*, Vol. 102-2, Advances in the Astronautical Sciences, American Astronautical Society, San Diego, CA, 1999, pp. 1333–1344.

[3]Estes, R., Lorenzini, E., Sanmartín, J., Peláez, J., Martínez-Sánchez, M., Johnson, L., and Vas, I., "Bare Tethers for Electrodynamic Spacecraft Propulsion," *Journal of Spacecraft and Rockets*, Vol. 37, No. 2, 2000, pp. 205–211.

[4]Johnson, L., and Ballance, J., "Propulsive Small Expendable Deployer System (ProSEDS) Space Demonstration," *Tether Technology Interchange Meeting*, NASA CP-1998-206900, Sept. 1997, pp. 109–129.

[5]Sanmartín, J., Martínez-Sánchez, M., Ahedo, E., "Bare Wire Anodes for Electrodynamic Tethers," *Journal of Propulsion and Power*, Vol. 9, No. 3, 1993, pp. 353–360.

[6]Martínez-Sánchez, M., and Hastings, D. E., "A Systems Study of a 100 kW Electrodynamic Tether," *Journal of the Astronautical Sciences*, Vol. 35, No. 1, 1987, pp. 75–96.

[7]Peláez, J., López-Rebollal, O., Ruiz, M., Lorenzini, E., Estes, R., and Cosmo, M., "On the Radial Oscillation of an Electrodynamic Tether," *Spaceflight Mechanics 1999*, Vol. 102-2, Advances in the Astronautical Sciences, American Astronautical Society, San Diego, CA, 1999, pp. 1361–1380.

[8]Peláez, J., Lorenzini, E., López-Rebollal, O., and Ruiz, M., "A New Kind of Dynamic Instability in Electrodynamic Tethers," *Journal of the Astronautical Sciences*, Vol. 48, No. 4, 2000, pp. 449–476.

[9]Levin, E. M.,"Stability of the Stationary Motions of an Electromagnetic Tether System in Orbit," *Cosmic Research*, Vol. 25, 1987, pp. 368–376.

[10]Beletsky, V., and Levin, E., *Dynamics of Space Tether Systems*, American Astronautical Society, San Diego, CA, 1993.

[11]Landau, L., and Lifshitz, E., *Mécanique*, Vol. 1, *Cours de Physique Théorique*, Mir, Moscow, 1982, p. 192.

[12]Wertz, J. R., *Spacecraft Attitude Determination and Control*, Vol. 73, Astrophysics and Space Science Library, Kluwer Academic, Dordrecht, The Netherlands, 1978, p. 783.

[13]Hartman, P., *Ordinary Differential Equations*, Birkhäuser, Boston, 1982, p. 60.

[14]Peláez, J., López-Rebollal, O., Ruiz, M., and Lorenzini, E. C., "Damping in Rigid Electrodynamic Tethers on Inclined Orbits," *Spaceflight Mechanics 2001*, edited by L. A. D'Amario, L. L. Sackett, D. J. Scheeres, and B. G. Williams, Vol. 2, No. 108, Advances in the Astronautical Sciences, American Astronautical Society, San Diego, CA, 2001, pp. 1209–1224.

[15]Ruiz, M., Lorenzini, E. C., Peláez, J., and López-Rebollal, O., "Modal Analysis of the Stability of Periodic Solutions in Electrodynamic Tethers," 2001 AAS/AIAA Astrodynamics Specialist Conf., American Astronautical Society Paper AAS 01-405, July–Aug. 2001.

[16]Corsi, J., Iess, L., "Stability and Control of Electrodynamic Tethers for De-Orbiting Applications," *Acta Astronautica*, Vol. 48, No. 5–12, 2001, pp. 491–501.

[17]Peláez, J., López-Rebollal, O., Lara, M., and Ahedo, E., "Dynamic Stability of a Bare Tether as a Deorbiting Device," 2002 AAS/AIAA Space Flight Mechanics Meeting, American Astronautical Society Paper AAS 02-200, Jan. 2002.